Synthesis of magnesium ferrite by combustion of glycine-nitrate gel: the influence of reagents on the gel-precursor and the microstructure of nanopowders

Maria N. Smirnova[1,a], Galina E. Nikiforova[1,b], Olga N. Kondrat'eva[1,c]

[1]Kurnakov Institute of General and Inorganic Chemistry of the Russian Academy of Sciences, Moscow, Russia

[a]smirnovamn@igic.ras.ru, [b]gen@igic.ras.ru, [c]olga.kondratieva@igic.ras.ru

Corresponding author: M. N. Smirnova, smirnovamn@igic.ras.ru

ABSTRACT In this study, the influence of initial reagents on the phase composition and morphology of magnesium ferrite obtained by combustion of glycine-nitrate gel was investigated. The local environment of iron ions in the gel-precursor was studied in detail using FT-IR, XANES- and EXAFS- spectroscopy. It has been established that in the gel-precursor obtained by dissolving metals (Mg, Fe) in dilute nitric acid, binuclear Fe(III) complexes are formed, while in a similar gel-precursor obtained from crystalline hydrates of nitrates of the corresponding metals, trinuclear Fe(III) complexes predominate. Combustion of a gel consisting of binuclear Fe(III) complexes leads to the formation of nanocrystalline magnesium ferrite powder, characterized by a unimodal particle size distribution.

KEYWORDS gel combustion, glycine, spinel, nanopowders, $MgFe_2O_4$

1. Introduction

Ferrites with a spinel structure have attracted the interest of researchers for many years due to their combination of magnetic and electrical properties, chemical and thermal stability, and low toxicity. One of the representatives of this class of compounds is magnesium ferrite $MgFe_2O_4$ – a soft magnetic semiconductor material that is used in heterogeneous catalysis, the production of sensors, microelectronics and medicine [1–6]. The magnetic characteristics of this ferrite, and therefore the possibility of its practical use, largely depend on the particle size, degree of crystallinity and morphological homogeneity. Depending on the synthesis method, these parameters can vary within wide limits. Various methods for producing ferrites with a spinel structure are described in the literature, among which the most common are the solid-phase synthesis [5, 7], the coprecipitation method [4, 8], the hydrothermal method [9, 10] and gel combustion method [11, 12].

The main advantage of the gel combustion method is the successful combination of chemical homogenization of the starting components through the use of complexing agents and the high-temperature short-term stage of the precursor gel combustion in a self-sustaining mode, which makes this method promising for the production of highly dispersed oxide powders. Currently, there is a significant number of publications that examine the influence of the choice of organic "fuel" (for example, citric acid, glycine, urea, etc.), as well as the ratio of the initial components of the reaction (excess, deficiency or stoichiometric amount of "fuel" in relation to metal compounds) on the phase composition of the final product [13–22]. However, intermediate stages of synthesis, such as the formation and structuring of gels, as well as the influence of these processes on the characteristics of the final product, have been little studied. At the same time, this information is necessary for the targeted production of oxide materials of a given composition with certain morphological characteristics.
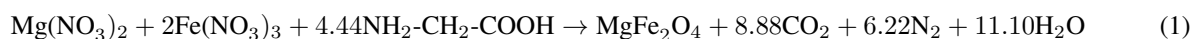
In this work, two approaches to the synthesis of magnesium ferrite $MgFe_2O_4$ by the gel combustion method were used and compared, one of which involves the preparation of an initial solution of nitrates by dissolving metallic magnesium and iron in dilute nitric acid, the second is based on the dissolution of crystalline hydrates of magnesium and iron nitrates in water. The purpose of this work is to study the structural features of precursor gels and to identify the existence of a connection between the choice of initial reagents and the phase and morphological properties of the final product.

2. Experimental

2.1. Synthesis MgFe$_2$O$_4$ from metals

An aqueous solution of magnesium (II) and iron (III) nitrates in a molar ratio of 1:2 was obtained by dissolving 0.279 g of metallic iron (Purissimum speciale), 0.061 g of metallic magnesium (Purissimum) in dilute (1:3) nitric acid. The number of metals was calculated so that the mass of the final product, that is MgFe$_2$O$_4$ powder, was 5 g.

To completely dissolve the metals and remove excess nitric acid, the solution was evaporated in a conical glass flask at a temperature of 80–90°C for 30 hours with constant stirring, regularly adding distilled water. The resulting nitrate solution "NM" (pH < 2) was further cooled, with an equivalent amount of glycine (0.833 g) added to it. To determine the equivalent ratio of the initial components, the balance between the valences of the oxidising and the reducing agent was used (the method of oxidising and reducing valences). Using this method, the energy released during the combustion of the mixture is assumed to be maximum when the ratio of the valence sum of the oxidising agent to the valence sum of the reducing agent is equal to one. According to calculations, 4.44 mol of glycine is required to produce 1 mol of MgFe$_2$O$_4$ (Eq. 1):

$$\text{Mg(NO}_3)_2 + 2\text{Fe(NO}_3)_3 + 4.44\text{NH}_2\text{-CH}_2\text{-COOH} \rightarrow \text{MgFe}_2\text{O}_4 + 8.88\text{CO}_2 + 6.22\text{N}_2 + 11.10\text{H}_2\text{O} \qquad (1)$$

The resulting reaction mixture was evaporated in an open porcelain cup (approximately 80–90°CC, for 2 hours) with constant stirring until it transformed into a gel (GM).

Subsequently, violent combustion occurred at a temperature of >100°C. Then, the powdered combustion product (PM) was kept for 30 minutes at a temperature of about 100–120°C, cooled, ground with a ball mill, and annealed at 700°C (for 6 h) in a muffle laboratory furnace.

2.2. Synthesis of MgFe$_2$O$_4$ from crystalline hydrates of metal nitrates

An aqueous solution of magnesium (II) and iron (III) nitrates in a molar ratio of 1:2 was obtained by dissolving 12.444 g of iron (III) nitrate nonahydrate and 3.756 g of magnesium (II) nitrate hexahydrate in distilled water. Before the synthesis, the water content in the crystal hydrates was specified by the gravimetric method. As a result, the number of the initial reagents was calculated for the following crystal hydrates (Fe(NO$_3$)$_3$·9.6 H$_2$O and Mg(NO$_3$)$_2$·5.7 H$_2$O so that the mass of the final product, that is MgFe$_2$O$_4$ powder, was 5 g.

After preparing the nitrate solution "NC" (pH $\sim$ 5), further steps of synthesis correspond to the procedure presented in Section 2.1. and include the preparation of the gel (GC), its combustion and annealing to form a powdery product (PC).

A summary scheme for synthesis of GM and GC, PM and PC samples is presented in Fig. 1.

2.3. Synthesis of iron nitrate gel (a sample-control)

To study the local atomic structure of gels by EXAFS spectroscopy, a sample-control (GF) was additionally prepared. The synthesis was carried out by dissolving metallic iron (Purissimum speciale) in dilute (1:3) nitric acid (the iron content is the same as in the sample "NM"). The resulting solution was repeatedly (5–8 times) evaporated in a conical glass flask at 80–90°C, adding distilled water regularly. Glycine was further added to the resulting solution in an equivalent amount that is required to obtain 5 g of Fe$_2$O$_3$ powder. This reaction mixture was evaporated until it transformed into a gel (GF).

2.4. Research methods

Chemical analysis of initial nitrate solutions, gels and powders was performed by inductively coupled plasma atomic emission spectrometry (ICP-AES) on an ICAP PRO XP spectrometer (Thermo Electron Corp., USA). Measurements were performed in the radial plasma view mode at the following spectrometer settings (power 1150 W, nebulizer gas flow 0.60 l/min, auxiliary gas flow 0.35 l/min, cooling gas flow 10 l/min).

FTIR spectra of gels and glycine were recorded on a Perkin Elmer Spectrum 65 FT-IR spectrometer in the region of 4000–400 cm^{-1} with a resolution of 2 cm^{-1}.

Iron K-edge EXAFS spectra were recorded in transmission mode by measuring the intensity of the X-ray beam before and after passing through the sample using argon-filled ionization chambers. For obtaining Fe K-edge spectra Si(111) channel-cut monochromator (energy resolution $\Delta E/E \approx 2 \times 10^{-4}$) and two ion chambers filled with argon were used. A standard processing of XAS spectra was carried out in terms of IFEFFIT software package [23, 24]. Normalized EXAFS oscillations were k^2- or k^3-weighted, Fourier transforms were taken in a 2.5–13.0Å^{-1} k-range. The Fourier-transformed EXAFS oscillations were fitted in the range of 1.2–3.8 Å. The amplitude reduction factor for iron was taken as 1.

The phase identity and purity of magnesium ferrite were confirmed by X-ray powder diffraction (XRD), using a Bruker D8 Advance XRD diffractometer equipped with Ni-filtered CuK$_{\alpha 1}$-radiation ($\lambda = 1.5406$ Å) and a LYNXEYE detector. The sample was scanned between 10°C and 60°C 2θ with a step size of 0.0133°C and a counting time of 0.5 s per step. In order to interpret the results of XRD experiments, a Bruker DIFFRAC.EVA software package and the ICDD PDF-2 database were used.

The surface morphology and microstructure of MgFe$_2$O$_4$ powders were investigated using a Carl Zeiss NVision 40 scanning electron microscope (SEM).
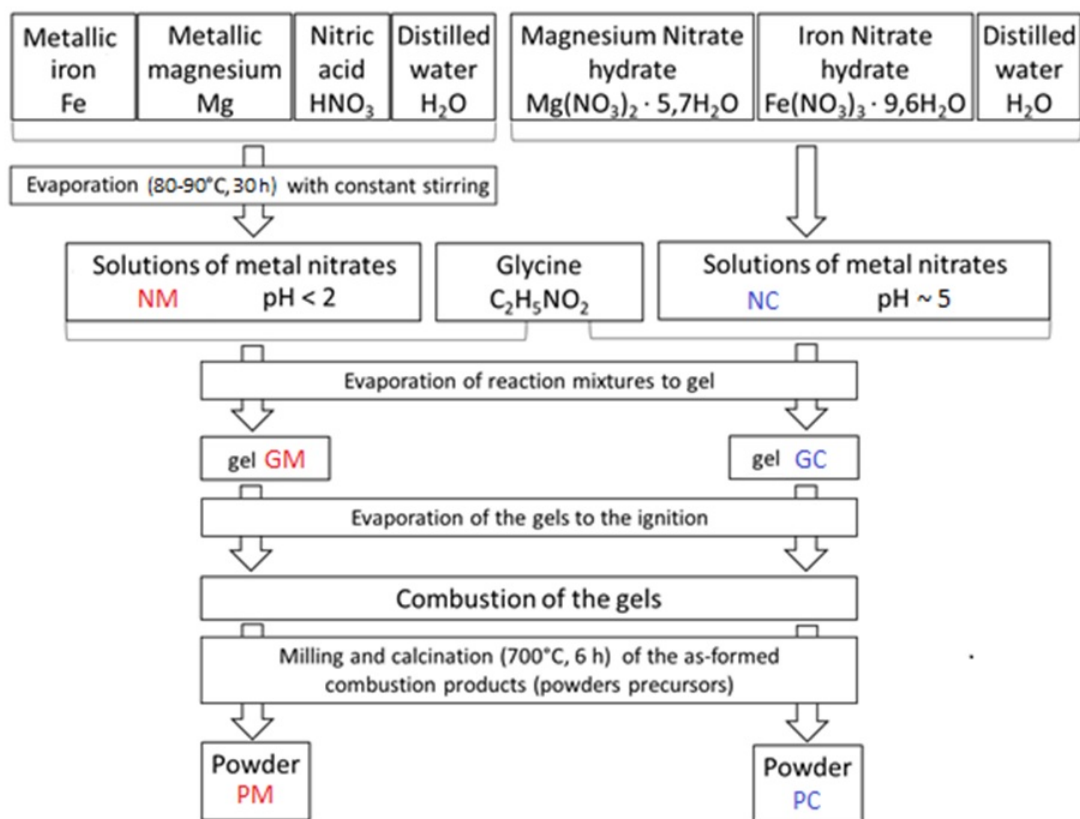
FIG. 1. Scheme of synthesis of gels (GM and GC) and powders (PM and PC)

3. Results and discussions

3.1. Elemental analysis of precursors and final product

The results of chemical analysis of precursors and finished powders are presented in Table 1. At all stages of synthesis for both samples, the ratio of elements remained constant and was close to the theoretical value. However, it should be noted that for the samples obtained from metal nitrates crystalline hydrates, a slight excess of magnesium is observed. It is likely that the use of crystalline hydrates of metal nitrates to prepare the initial solution, due to their hygroscopicity, can lead to deviations from the specified ratios of metal cations.

TABLE 1. Results of elemental analysis of nitrate solutions (NM and NC), gels (GM and GC) and powders (PM and PC)

Sample	Theoretical		Experimental	
	Mg, % wt.	Fe, % wt.	Mg, % wt.	Fe, % wt.
NM			17.9	82.1
GM			17.5	82.5
PM	17.6	82.4	17.6	82.4
NC			18.0	82.0
GC			18.1	81.9
PC			18.2	81.8

3.2. FTIR spectral analysis

To identify the role of the functional groups of the reagents in the process of formation of the structure of the gels, their Fourier transform IR spectra were initially studied, as well as the spectra of the starting glycine for comparative analysis (Fig. 2).
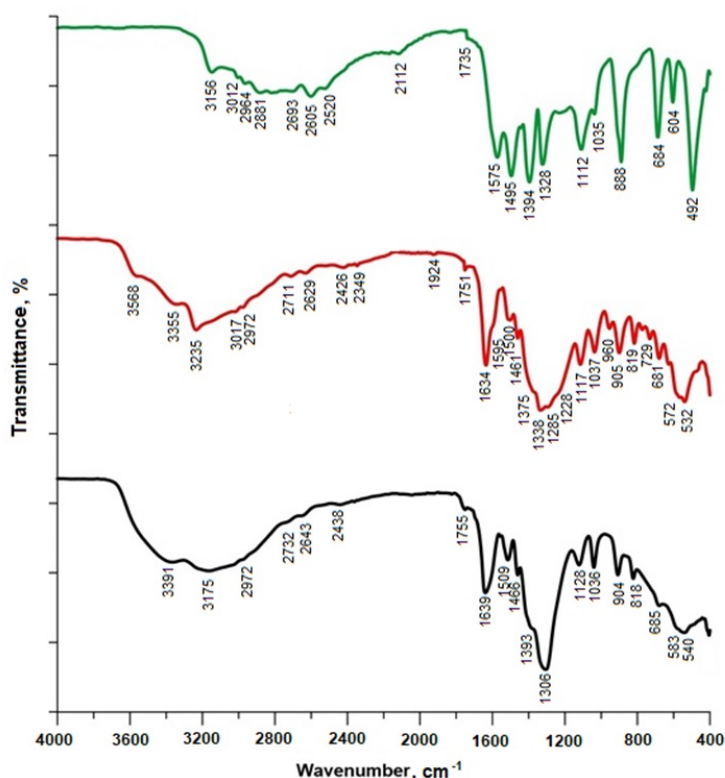
FIG. 2. FTIR spectra (from top to bottom) of glycine, GM and GC gels

The FTIR spectrum of glycine corresponds to the standard spectrum of γ-glycine [25]. The intense absorption peak at 492 cm^{-1} is due to torsional vibrations of the amino group. The bands at 604 cm^{-1} and 684 cm^{-1} are associated with bending vibrations of the COO$^-$ group. The C–C stretching vibration produced absorption bands at 888 cm^{-1}. The peak at 1328 cm^{-1} can be attributed to both the wagging vibrations of CH$_2$ groups [26] and the bending vibrations of the methylene and amino groups [27]. Weak bands traced at 1035 cm^{-1} and 1112 cm^{-1} are due to C–N stretching vibrations. Three bands characteristic of the zwitterionic nature of amino acids are further observed at 1394 cm^{-1} (symmetric stretching of COO$^-$ groups), 1495 cm^{-1} (symmetric bending of NH^{3+} ions) and 1575 cm^{-1} (asymmetric stretching of COO$^-$ groups). In the range 2500–3200 cm^{-1}, broad bands due to symmetric and asymmetric stretching vibrations of N–H and C–H bonds are observed [26–29].

The general appearance of the FTIR spectra of GM and GC gels differs from the spectrum of glycine. In both spectra there is no band at 492 cm^{-1}, which indicates binding of the nitro group. Moreover, additional absorption bands appear: in the region of 500–600 cm^{-1}, associated with stretching vibrations of the Mg-O and Fe-O bonds, as well as bands located at 819 cm^{-1} and in the region of 1450–1300 cm^{-1}, which is associated with bending vibrations of the NO$_3^-$ group and stretching vibrations of N–O bonds [30, 31]. The position of the bands indicates a distortion of the geometry of free nitrate ions. In this case, the magnitude of the frequency separation of the bands ($\Delta\nu$) is different, which indicates the presence in the gels of nitrate groups with different types of bonds – coordination and ionic. The pronounced spectral absorption band at 1634–1639 cm^{-1} is associated with bending vibrations of the H–O–H bond of water. The FTIR region of 3000–3600 cm^{-1} indicates the presence of OH- groups in the gels involved in the formation of hydrogen bonds. It is difficult to make more precise conclusions about the nature of the bonds, since in this region the bands of stretching vibrations of OH-groups, amino-groups and the N(H)...O hydrogen bond overlap. It should be noted that for the GM gel, the above absorption bands are shifted towards higher frequencies, which indicates the formation of weaker hydrogen bonds compared to the GC gel. Another important difference in the FTIR spectra of the gels is the presence in the spectrum of the GM gel of two absorption bands at 1228 cm^{-1} and 1298 cm^{-1}, associated with vibrations of the carboxyl group and characteristic only of the cationic form of glycine [27].

3.3. X-ray Absorption Spectroscopy

At the next step of investigation GM and GC gels were studied by XAS-spectroscopy (Fig. 3). This method allows obtaining structural information of nearest environment of iron atoms in organometallic gels. For a more accurate interpretation of the results, a control sample marked as GF was additionally prepared.

The XANES spectra (Fig. 3a) of samples GC, GM and GF are almost coincident, which indicates that iron is in an octahedral environment in all gels. The most intense peak at the range of $\sim$1–2 Å on the R-δ scale in the EXAFS data
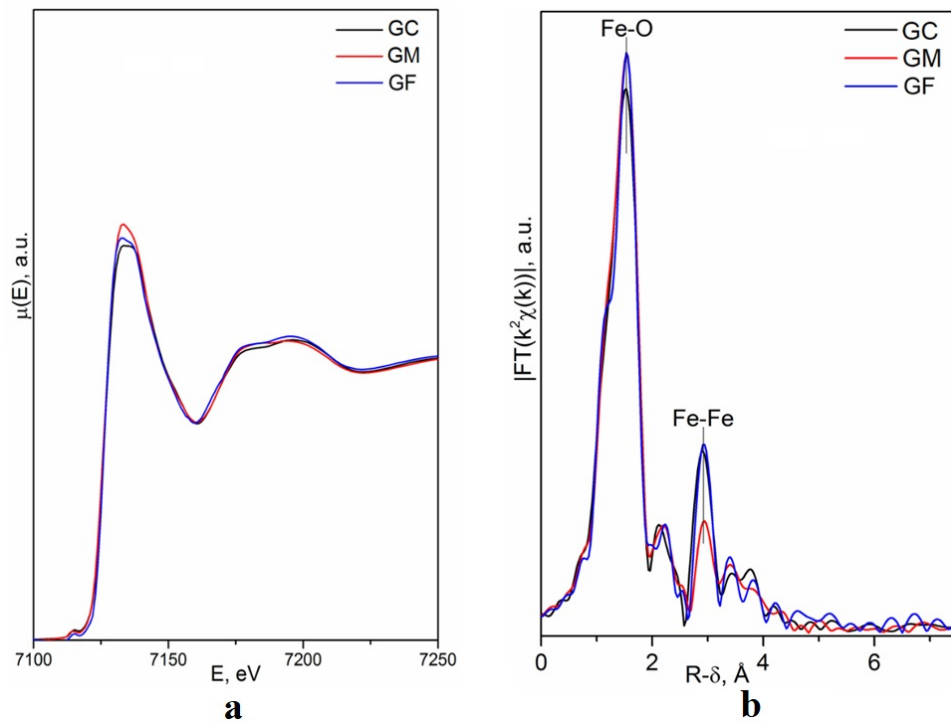
FIG. 3. XANES spectra (a) and EXAFS Fourier transforms (b) of iron K edge for organometallic gels GC, GM and GF
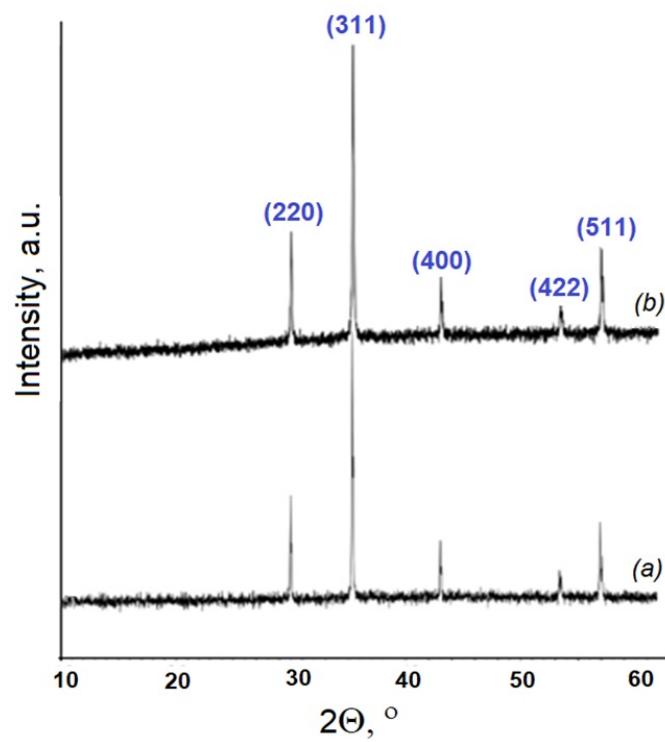

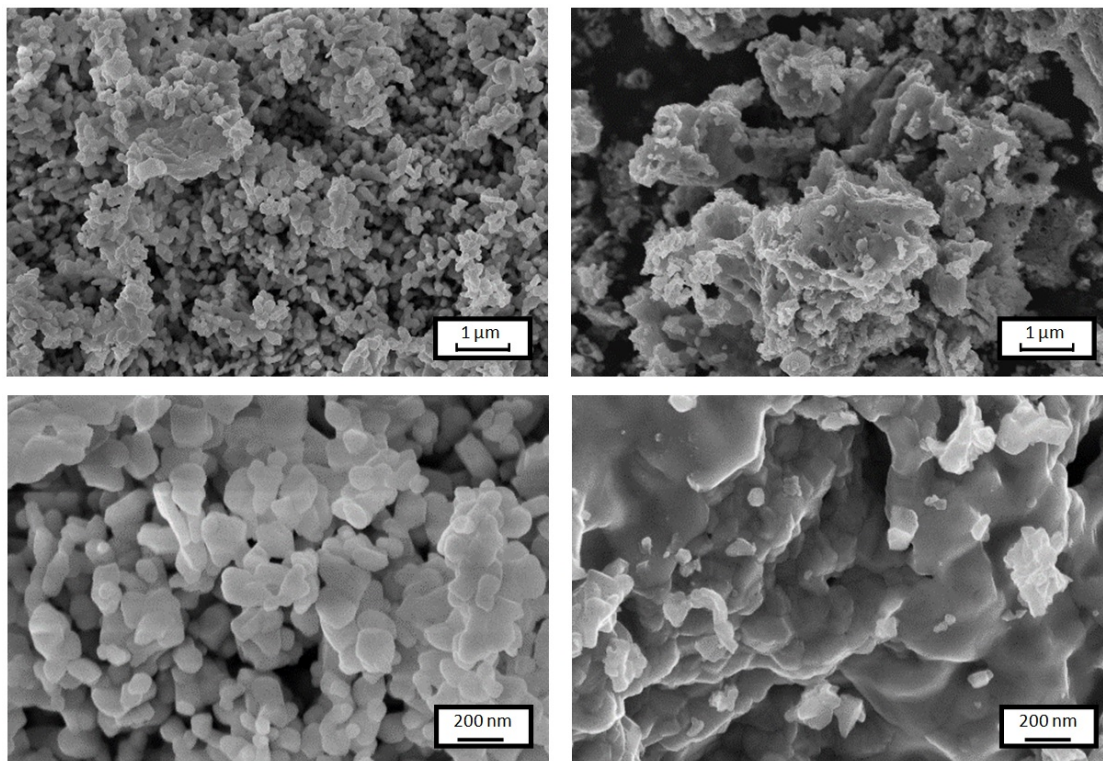FIG. 4. X-ray diffraction patterns of PM (a) and PC (b) powders

FIG. 5. SEM images of $MgFe_2O_4$ nanopowders (PM on the left and PC on the right) after annealing at $700°C$

(Fig. 3b) refers to the oxygen atoms of the first coordination sphere of iron. The less intense peak (R $\sim$3 Å) corresponds to the Fe atoms (Fig. 3b). The simulation results for the reference sample GF (Table 2) indicate the formation of a trinuclear iron (III) complex with glycine [32]. There are 6 oxygen atoms in the first coordination sphere of iron ($\sim$1.9–2.0 Å) and two equidistant iron atoms at a distance of $\sim$3.31 Å in the structure of this complex (Table 2).

Applying the parameters of this model to the EXAFS data of GM and GC samples shows that the GC gel contains an iron (III) complex similar to that described above. However, in the case of the GM sample some differences are observed: the number of oxygen atoms in the first coordination sphere remains the same, but in the second coordination sphere the coordination number (CN) of iron decreases from two to one (Table 2).

It can be assumed that in the case of the GM sample, an iron complex of a slightly different composition is formed. Also, the decrease in the CN in the coordination sphere of Fe-Fe at 3.31 Å from 2 to 1 may possibly be associated with the formation of a binuclear Fe(III) complex in the GM sample, which differs in structure from the trinuclear Fe(III) complex in the GC gel.

One possible explanation for the observed difference in the structure of GM and GC gels is the acidity of glycine-nitrate solutions prepared from metals and nitric acid (NM) or metal crystalline hydrates (NC). In NM solution at pH$\leq$2, glycine is present predominantly in a protonated (cationic) form ($H_3N^+CH_2COOH$), which is not prone to forming complexes with metal cations. Probably, the binding of metal cations occurs through hydroxyl groups. On the other hand, the formation of the gel structure in the GC sample occurs from a weakly acidic solution with pH$\sim$5, in which glycine is present in a more reactive form (zwitterion), which leads to the formation of a trinuclear Fe(III) complex.

3.4. XRD and SEM analysis of powders

PM and PC powders obtained after combustion the gels were heat treated in air at a temperature of $700°C$ for 6 hours and then investigated by XRD and SEM. According to X-ray phase analysis (Fig. 4), both powders are magnesium ferrite with a spinel structure (Fd-$3m$ space group). No reflections of impurity phases were detected. Crystallographic parameters of $MgFe_2O_4$ (Table 3) were found to be in a good agreement with the data of ICDD (PDF 04-012-0908, PDF 04-010-6157, PDF 04-006-6673).

The average crystallite size d_{XRD} was estimated using Scherrer's equation:

$$d_{XRD} = \frac{K \cdot \lambda}{\beta \cdot \cos\theta}, \tag{2}$$

where K is the shape factor (0.9), λ is the X-ray wavelength (0.15418 nm), θ is the diffraction angle and β is the full width at half-maximum (FWHM) intensity of the diffraction line.

TABLE 2. Fit results for the EXAFS data for the iron gels: R – interatomic distance, CN – coordination number, σ^2 – Debye factor, R – matching factor between the experimental and model spectra. Fixed parameters are marked with *, equal values designated by ”

Sample	Scattering atom	CN	σ^2, Å^2	R, Å (model)	R, Å (from EXAFS data)	R_f, %
GF	O	3.0*	0.0043”	1.91	1.97	1.1
	O	3.0*	0.0043”	2.03	2.07	
	C	2.0*	0.0169”	2.98	3.11	
	C	2.0*	0.0169”	2.98	3.31	
	Fe	2.0*	0.0155	3.31	3.44	
	O	2.0*	0.0048”	3.32	3.47	
	O	2.0*	0.0048”	3.46	3.60	
	O	2.0*	0.0004	3.80	3.80	
	O	2.0*	0.0026	4.00	4.23	
GC	O	1.0*	0.0011	1.92	1.90	1.7
	O	5.0*	0.0047	2.03	2.03	
	C	3.1	0.0056	2.98	3.00	
	Fe	2.0*	0.0061	3.31	3.31	
	O	2.1	0.0050	3.80	3.76	
GM	O	4.0*	0.0040	1.92	1.98	1.8
	O	2.0*	0.0027	2.03	2.09	
	C	2.0*	0.0049	2.98	3.01	
	Fe	1.0*	0.0079	3.31	3.34	
	O	2.0*	0.0115	3.80	3.71	

TABLE 3. Unit cell parameters and crystalline size values for PM and PC powders

Sample	a, nm	V, nm^3	d_{XRD}, nm
PM	0.8380(3)	0.5885(4)	102(3)
PC	0.8391(5)	0.5908(4)	89(7)

According to SEM data (Fig. 5), PM powder consists of spherical particles 50–120 nm in size, weakly agglomerated. PC powder, on the contrary, contains large agglomerates of particles that are heterogeneous in morphology and size. This morphological difference is likely a consequence of structural differences between GM and GC gels. Probably, the structure of the GM gel ensures a uniform distribution of metal cations and is instantly destroyed upon combustion of the gel with the formation of a homogeneous nanopowder of magnesium ferrite. The authors of [30] also noted that the combustion of a glycine-nitrate gel consisting of mononuclear complexes led to the formation of a more highly dispersed powder compared to the results of combustion of a gel consisting of six-nuclear complexes.

4. Conclusion

In this study, we showed how the choice of starting reagents as well as the precursor preparation approach influences the gel structure and morphology of the final magnesium ferrite powder. The formation of GM gel, the initial nitrate solution for which was prepared by dissolving metals in nitric acid, as shown by spectroscopic studies, occurs without pronounced complex formation between glycine and metal cations. Homogenization of the starting components occurs due to the formation of aqua complexes - a system of "weak" ionic and hydrogen bonds. Such a gel is simultaneously

destroyed during the combustion process with the formation of a homogeneous magnesium ferrite powder of a given stoichiometry, the morphological features of which are characterized by nano-sized particles that are not prone to aggregation and have a uniform distribution of their sizes.

The structuring of the GC gel, for which the initial nitrate solution was an aqueous solution of metal nitrate hydrates, is largely associated with the formation of organometallic complexes. The decomposition of these complexes is probably divided in time and has a multi-stage nature, which leads to morphological heterogeneity of the final product.

Thus, the choice of initial reagents has a significant impact on the morphology of iron-magnesium ferrite particles with a spinel structure. The information obtained on the mechanisms of structuring of glycine-nitrate metal-containing gels expands the understanding of the possibilities of targeted synthesis for obtaining complex metal oxides with a given set of properties and characteristics.

References

[1] Heidari P., Masoudpanah S.M. Structural and magnetic properties of $MgFe_2O_4$ powders synthesized by solution combustion method: the effect of fuel type. *J. Mater. Res. Technol.*, 2020, **9**(3), P. 4469–4475.

[2] Nagarajan V., Thayumanavan A. $MgFe_2O_4$ thin films for detection of ethanol and acetone vapours. *Surf Eng*, 2018, **34**(9), P. 711–720.

[3] Polat K., Yurdakoc M. Solar Decolorization of Methylene Blue by Magnetic $MgFe_2O_4$-MWCNT/Ag_3VO_4 Visible Active Photocatalyst. *Water Air Soil Pollut.*, 2018, **229**, P. 331.

[4] Liming F., Haowen C., Kang W., Xitao W. Oxygen-vacancy generation in $MgFe_2O_4$ by high temperature calcination and its improved Photocatalytic activity for CO_2 Reduction. *J. Alloys Compd.*, 2021, **891**, P. 161925.

[5] Das K.Ch., Dhara S.S. Rapid catalytic degradation of malachite green by $MgFe_2O_4$ nanoparticles in presence of H_2O_2. *J. Alloys Compd.*, 2020, **828**(5), P. 154462.

[6] Nadargi D., Umar A., Nadargi J., Patil J., Mulla I., Akbar S., Suryavanshi S. Spinel Magnesium Ferrite ($MgFe_2O_4$): A Glycine-Assisted Colloidal Combustion and Its Potentiality in Gas-Sensing Application. *Chemosensors*, 2022, **10**(9), P. 361.

[7] Zhang L., Wang Y., Liu B., Wang J., Han G., Zhang Y. Characterization and property of magnetic ferrite ceramics with interesting multilayer structure prepared by solid-state reaction. *Ceram. Int.*, 2021, **47**(8), P. 10927–10939.

[8] Naaz F., Dubey H. K., Kumari C., Lahiri P. Structural and magnetic properties of $MgFe_2O_4$ nanopowder synthesized via co-precipitation route. *SN Applied Sciences*, 2020, **2**(5), P. 808.

[9] Naidu K.C.B., Madhuri W. Microwave Hydrothermal Synthesis: Structural and Dielectric Properties of nano $MgFe_2O_4$. *Materials Today: Proceedings*, 2016, **3**(10 B), P. 3810–3813.

[10] Mishra B., Munisha B., Nanda J., Sankaran K.J., Suman S. Hydrothermally Synthesized Magnesium doped Zinc Ferrite Nanoparticles: An extensive study on structural, optical, magnetic, and dielectric properties, *Materials Chemistry and Physics*, 2022, **292**, P. 126791.

[11] Komlev A.A., Gusarov V.V. Glycine-nitrate combustion synthesis of nonstoichiometric Mg-Fe spinel nanopowders. *Inorg Mater.*, 2014, **50**, P. 1247–1251.

[12] Zhernovoi A.I., Komlev A.A., D'yachenko S.V., Magnetic characteristics of $MgFe_2O_4$ nanoparticles obtained by glycine–nitrate synthesis. *Tech. Phys.*, 2016, **61**, P. 302–305.

[13] Jamdade S., Tambade P., Rathod S., Structural and magnetic study of Tb^{3+} doped zinc ferrite by sol-gel auto-combustion technique. *Nanosyst. Physics, Chem. Math.*, 2023, **14**, P. 254–263.

[14] Varma A., Mukasyan A.S., Rogachev A.S., Manukyan K.V. Solution combustion synthesis of nanoscale materials, *Chemical Reviews*, 2016, **116**, P. 14493–14586.

[15] Carlos E., Martins R., Fortunato E., Branquinho R. Solution combustion synthesis: towards a sustainable approach for metal oxides. *Chem.–Eur. J.*, 2020, **26**, P. 9099–9125.

[16] Wen W., Wu J.-M. Nanomaterials via solution combustion synthesis: a step nearer to controllability. *RSC Adv.*, 2014, **4**, P. 58090.

[17] Li F.-T., Ran J., Jaroniec M., Qiao S.Z. Solution combustion synthesis of metal oxide nanomaterials for energy storage and conversion. *Nanoscale*, 2015, **7**, P. 17590–17610.

[18] Smirnova M.N., Glazkova I.S., Nikiforova G.E., Kop'eva M.A., Eliseev A.A., Gorbachev E.A., Ketsko V.A., Synthesis of Ce:YIG nanopowder by gel combustion, *Nanosyst. Physics, Chem. Math.*, 2021, **12**(2), P. 210–217.

[19] Zhuravlev V.D., Dmitriev A.V., Vladimirova E.V. et al. Parameters of Glycine–Nitrate Synthesis of $NiCo_2O_4$ Spinel. *Russ. J. Inorg. Chem.*, 2021, **66**, P. 1895–1903.

[20] Martinson K.D., Belyak V.E., Sakhno D.D., Kiryanov N.V., Chebanenko M.I., Popkov V.I., Effect of fuel type on solution combustion synthesis and photocatalytic activity of $NiFe_2O_4$ nanopowders. *Nanosyst. Physics, Chem. Math.*, 2021, **12**, P. 792–798.

[21] Lebedev L. A., Tenevich M. I., Popkov V. I. The effect of solution-combustion mode on the structure, morphology and size-sensitive photocatalytic performance of $MgFe_2O_4$ nanopowders. *Condensed Matter and Interphases*, 2022, **24**(4), P. 496–503.

[22] Mukasyan A.S., Rogachev A.S., Aruna S.T., Combustion synthesis in nanostructured reactive systems. *Adv. Powder Technol.*, 2015, **26**, P. 954–976.

[23] Ravel B., Newville M. ATHENA, ARTEMIS, HEPHAESTUS: data analysis for X-ray absorption spectroscopy using IFEFFIT. *J. Synch. Radiat*, 2005, **12**(4), P. 537–541.

[24] Newville M. IFEFFIT: interactive XAFS analysis and FEFF fitting. *J. Synch. Radiat.*, 2001, **8**(2), P. 322–324.

[25] https://webbook.nist.gov/cgi/cbook.cgi?ID=C56406&Units=SI&Type=IR-SPEC&Index=1#IR-SPEC

[26] Silverstein R.M., Bassler G.C., Morrill T.C. *Spectrometric Identification of Organic Compounds*, John Wiley & Sons, New York, 1981.

[27] Butyrskaya E.V., Nechaeva L.S., Shaposhnik V.A., Drozdova E.I. Assignment of bands in IR spectra of aqueous glycine solutions based on quantum chemical calculation. *J. Sorption and chromatographic processes*, 2012, **12**(4), P. 501–511.

[28] Boldyreva E.V., Drebushchak V.A., Drebushchak T.N., Paukov I.E., Kovalevskaya Y.A., Shutova E.S. Polymorphism of glycine: Thermodynamic aspects. Part I - Relative stability of the polymorphs. *J. Therm. Anal. Calorim.*, 2003, **73**, P. 409–418.

[29] Larkin P. *Infrared and Raman Spectroscopy: Principles and Spectral Interpretation*, Elsevier, 2017, 286 p.

[30] Jain D., Sudarsan V., Patra A.K., Sastry P.U., Tyagi A.K. Effect of local ordering around Th^{4+} ions in glycine-nitrate precursor gel on the powder characteristic of gel-combusted ThO_2. *J. Nucl. Mater.*, 2019, **527**, P. 151826.

[31] Warrier A.V.R., Narayanan P.S. Infrared absorption spectra of single crystals of glycine silver nitrate and monoglycine nitrate. *Proc. Indian Acad. Sci.*, 1967, **66**, P. 46–54.

[32] Turte K.I., Lazaresku A.G., Simonov Yu.A., Lipkovskii Ya., Dvorkin A.A., Patron L. Structure of (μ_3-Oxo)-hexa(μ-glycine-O, O')triaquatriiron (III) Nitrate 3.5-Hydrate. *Russ. J. Coord. Chem.*, 1996, **22**(1), P. 45–53.

Information about the authors:

Maria N. Smirnova – Kurnakov Institute of General and Inorganic Chemistry of the Russian Academy of Sciences, 119991, 31 Leninsky Prospect, Moscow, Russia; ORCID 0000-0003-2707-7975; smirnovamn@igic.ras.ru

Galina E. Nikiforova – Kurnakov Institute of General and Inorganic Chemistry of the Russian Academy of Sciences, 119991, 31 Leninsky Prospect, Moscow, Russia; ORCID 0000-0002-2892-6054; gen@igic.ras.ru

Olga N. Kondrat'eva – Kurnakov Institute of General and Inorganic Chemistry of the Russian Academy of Sciences, 119991, 31 Leninsky Prospect, Moscow, Russia; ORCID 0000-0003-2508-9868; olga.kondratieva@igic.ras.ru